On the relationship between drag and vertical velocity fluctuations in flow over riblets and liquid infused surfaces

4 authors, including:

Simone Di Giorgio
CNR-INM
7 PUBLICATIONS   **39** CITATIONS

SEE PROFILE

Sergio Pirozzoli
Sapienza University of Rome
179 PUBLICATIONS   **4,910** CITATIONS

SEE PROFILE

Paolo Orlandi
Sapienza University of Rome
243 PUBLICATIONS   **7,727** CITATIONS

SEE PROFILE

Some of the authors of this publication are also working on these related projects:

Project   decaying turbulence View project

Project   heat transfer View project

On the relationship between drag and vertical velocity fluctuations in flow over riblets and liquid infused surfaces

Simone Di Giorgio[a,*], Stefano Leonardi[b], Sergio Pirozzoli[a] and Paolo Orlandi[a]

[a]*Dipartimento di Ingegneria Meccanica e Aerospaziale*
Sapienza Università di Roma
Via Eudossiana 18, 00184, Roma
[b]*Department of Mechanical Engineering, University of Texas at Dallas*
800 West Campbell Rd., Dallas, TX

ARTICLE INFO

ABSTRACT

Direct numerical simulations (DNS) of flow over triangular and rectangular riblets in a wide range of size and Reynolds number have been carried out. The flow within the grooves is directly resolved by exploiting the immersed-boundary method. It is found that the drag reduction property is primarily associated with the capability of inhibiting vertical velocity fluctuations at the plane of the crests, as in liquid-infused surfaces (LIS) devices. This is mimicked in DNS through artificial suppression of the vertical velocity component, which yields large drag decrease, proportionate to the riblets size. A parametrization of the drag reduction effect in terms of the vertical velocity variance is found to be quite successful in accounting for variation of the controlling parameters. A Moody-like friction diagram is thus introduced which incorporates the effect of slip velocity and a single, geometry-dependent parameter. Reduced drag-reduction efficiency of LIS-like riblets is found as compared to cases with artificially imposed slip velocity. Last, we find that simple wall models of riblets and LIS-like devices are unlikely to provide accurate prediction of the flow phenomenon, and direct resolution of flow within the grooves in necessary.

1. Introduction

Drag reduction is one of the primary goals in engineering fluid dynamics design, and viscous drag in particular is the primary driving factor for aircraft or marine vessels fuel consumption. Previous studies have suggested that micro-surface features which change the near-wall structure of the turbulent flow are effective in reducing drag, as is the case of riblets [22]. Choi et al. [4] carried out direct numerical simulation (DNS) of turbulent flows over riblet-mounted surfaces, achieving 6% drag reduction with triangular riblets with spanwise spacing in wall units $s^+ \approx 20$, and drag increase with $s^+ \approx 40$. They attributed the drag reduction effect to reduction of Reynolds stress near the riblets which prevents the cross-flow motion. García-Mayoral and Jiménez [7] claimed that good characterization of the riblets performance breakdown may be obtained using the groove cross-sectional area A_g, rather than the riblets spacing. In particular, they asserted that optimal performance of riblets is achieved for $\ell_g^+ = \sqrt{A_g} \approx 11$, regardless of the riblets shape. Many geometries and sizes of riblets have been studied numerically and experimentally, and maximum drag reduction is achieved of about 9%. The best results are typically obtained with sharp, blade-shaped riblets, which however are difficult to construct and maintain at the Reynolds numbers of engineering interest.

A strategy has been pursued in recent years to overcome the performance limit of riblets, which involves the use of super-hydrophobic surfaces [SHS, 12] and liquid-infused sur-faces [LIS, 1]. The effects of SHS on skin-friction drag have been investigated through direct numerical simulation of turbulent channel flow [12] [5], in which the actual surface texture is replaced with artificialy enforcement of a slip length $\ell_s = u/(\partial u/\partial y)$ at the wall. It was shown that imposing a slip velocity in the streamwise and in the spanwise directions has quite a different effect on the near-wall turbulence, resulting in large drag reduction in the former case and large drag increase in the latter case. Martell et al. [11] studied the variation of wall shear stress and Reynolds stresses in turbulent channel flow for a variety of SHS textures considering only the flow above the texture, by applying the no-slip condition at the top surface of each microfeature, and the free-slip condition at the suspended liquid–gas interface. Subsequently, Rastegari and Akhavan [20] derived a relation between the amount of drag reduction and the slip velocity, i.e. the average velocity on the texture. Arenas et al. [1] carried out DNS of turbulent channel flow with two superposed fluids having different viscosity, accounting for flow within the grooves. Different textured surfaces were considered, with several values of the viscosity ratio. Large drag reduction was obtained with staggered cubes patterns, which was connected with suppression of the wall-normal velocity fluctuations at the tip of the cubes. The importance of wall-normal velocity fluctuations in wall turbulence was previously emphasized by Orlandi and Leonardi [16], who connected the drag increase effect in flow over rough walls with the variance of the vertical velocity at the plane of crests.

In this work we carried out DNS in a turbulent channel flow with triangular and rectangular riblets at the lower wall, in which the flow within the grooves is directly resolved. Numerical simulations were carried out by changing the riblets

---

*Corresponding author
✉ simone.digiorgio@uniroma1.it (S. Di Giorgio)
ORCID(s):

size and/or the bulk Reynolds number, and by suppressing the vertical velocity at the plane of crests, especially mimicking LIS with unit viscosity ratio. Besides a general study of turbulence modification due to the presence of riblets, we aim at establishing whether a similar relationship between vertical velocity fluctuations and drag variation (with respect to the reference case of a smooth channel) as introduced by Orlandi and Leonardi [16] for rough surfaces can also be traced in SHS and/or LIS. For that purpose, we expand the study of Arenas et al. [1] for a broader database, spanning both roughness and ideal LIS. We further present a relationship between the roughness function and the slip velocity which is used to derive a Moody-like diagram for both drag increasing and drag reducing surfaces.

2. Methodology

The flows under scrutiny are governed by the incompressible Navier-Stokes and continuity equations,

$$\frac{\partial U_i}{\partial t} + \frac{\partial U_i U_j}{\partial x_j} = -\frac{\partial P}{\partial x} + \frac{1}{Re}\frac{\partial^2 U_i}{\partial x_j^2} + \Pi \delta_{i1}, \qquad (1)$$

$$\frac{\partial U_i}{\partial x_i} = 0, \qquad (2)$$

where the U_i's are the velocity components in the streamwise, wall-normal and spanwise directions, respectively, hereafter also referred to as U, V, W, Π is the pressure gradient required to maintain a constant flow rate and P is the pressure. The numerical method relies on second-order finite-difference discretization on a staggered mesh with direct inversion of Poisson equation for the pseudo-pressure [14], which accommodates arbitrarily complex geometries through the immersed-boundary method. As proposed by Orlandi and Leonardi [15], the no-slip condition at solid walls is indirectly enforced by re-defining the metrics for viscous derivative evaluation at the first layer of interface fluid points.

The computational box is $\pi h \times 2h \times 1.25h$ in the streamwise, wall-normal and spanwise directions, for all cases. Simulations are performed with a constant mass flow rate, at bulk Reynolds number in the range $Re_b = 3,500 - 20,000$. The upper boundary is assumed to be flat, and riblets are only placed at the lower wall, see Fig. 1. Triangular riblets with spanwise spacing $s = 0.125h$ and tip opening angle $\beta = 50.97°$ are considered as baseline geometry (T1), for which a mesh with $256 \times 512 \times 512$ points is used, with resolution $\Delta x^+ \approx 6.9$, $\Delta z^+ \approx 1.4$ at $Re_b = 20,000$. Additional simulations, denoted as T2, have been carried out at fixed $Re_b = 5,600$, for geometrically similar triangular riblets with various spanwise spacing, $s = 0.0415h, 0.083h, 0.166h$ (corresponding to $\ell_g = 0.03h, 0.06h, 0.12h$), on a $64 \times 384 \times 512$ mesh. Simulations of rectangular bars with same spacing and height (hence with same gas fraction) as the T1 riblets have also been carried out using the same domain and grid, and referred to as B in the following (see Fig. 2(a)). A list of selected flow conditions is given in Tab. 1. All DNS were
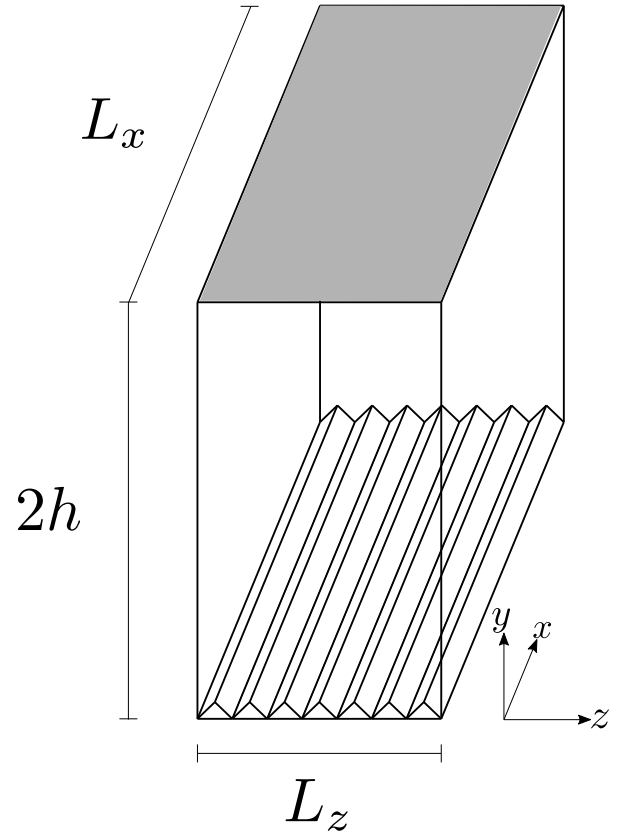

Figure 1: Computational domain with riblets at the lower wall.

repeated by artificially forcing zero vertical velocity at the plane of crests, to mimic conditions encountered in SHS or LIS with large surface tension, which are referred to with the $V0$ suffix in the following (see Fig. 2(a)). In all cases, flow within the grooves is directly resolved.

To a first approximation, suppression of the vertical velocity amounts to replacing the no-slip boundary condition at the lower wall with an axial velocity slip, which is in general non-uniform along the spanwise direction, and which depends on the riblets shape and on the Reynolds number. To verify whether this approximation is correct, we have carried out a series of companion DNS of Couette-Poiseuille-like flow [18], by assuming smooth lower wall with imparted slip velocity (U_0, see Fig. 2(b)). Cases with uniform slip velocity have been simulated, with $U_0 = 0.025 - 0.2U_b$, and $Re_b = 4,000 - 15,000$, which are referred to as CP. Cases with artificial sinusoidal spanwise variation of the slip velocity according to $U_0 = A \sin^2(\pi x/s)$, to more closely replicate the mean velocity distribution observed in triangular riblets, which are referred to as SIN. The mean slip velocity in this case is set to $U_0 = 0.1U_b$, with $Re_b = 4,000 - 15,000$. A mesh with $256 \times 384 \times 128$ is used for all these cases, listed in Tab. 2. In the following discussion, the reference case of flow in smooth channel with stationary walls is hereafter referred to as SM.
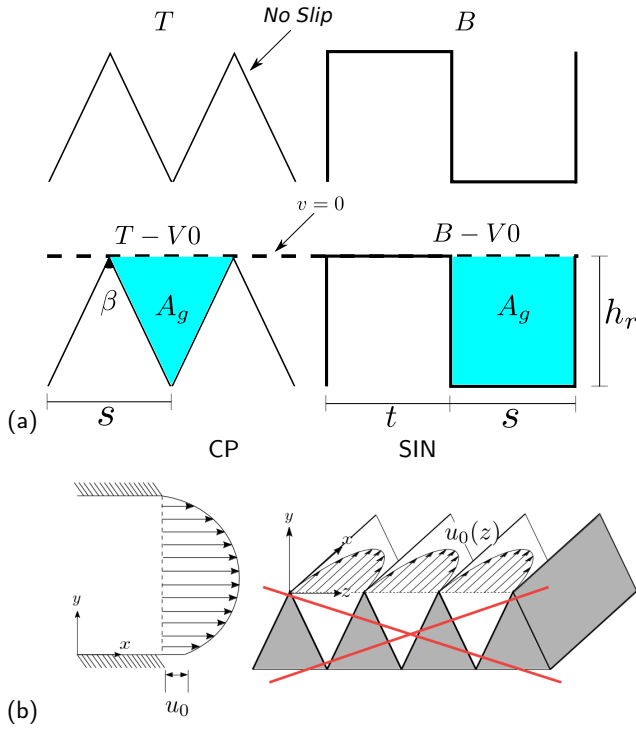
Figure 2: (a) Cross-stream geometry of triangular (T, left) and rectangular (B, right) riblets. For cases denoted with the $V0$ suffix zero vertical velocity ($V = 0$) is imposed at the plane of crests, marked with a dashed line. (b) Set-up of of companion Couette-Poiseuille simulations, with imparted slip velocity at the lower smooth wall $u_0(z)$.

Table 1
List of simulations done with riblets.

Name	Geometry	Re_b	h_r/h	s/h
T1	Triangular	3,500	0.125	0.131
T1	Triangular	5,000	0.125	0.131
T1	Triangular	10,000	0.125	0.131
T1	Triangular	15,000	0.125	0.131
T1	Triangular	20,000	0.125	0.131
T2	Triangular	5,600	0.0625	0.0656
T2	Triangular	5,600	0.125	0.131
T2	Triangular	5,600	0.250	0.262
B	Rectangular	3,500	0.125	0.131
B	Rectangular	5,000	0.125	0.131
B	Rectangular	10,000	0.125	0.131
B	Rectangular	15,000	0.125	0.131
B	Rectangular	20,000	0.125	0.131

3. Results

3.1. Drag reduction

Fig. 3 shows the relation between the percent drag reduction, $DR = 1 - \tau_{wr}/\tau_{ws}$, and the typical groove length scale, ℓ_g^+, where τ_{wr} and τ_{ws} are the wall shear stress at the lower and upper wall, respectively, the former being estimated from momentum balance. For the T1 and T2 test cases, our results are consistent with classical analysis [7]. In particular, maximum drag reduction is observed for $\ell_g^+ \approx$

Table 2
List of simulations done with slip-condition.

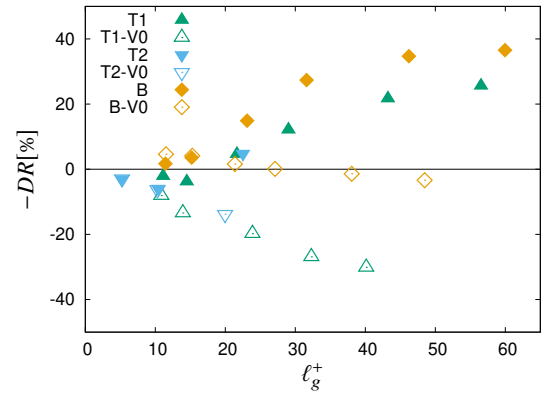| Name	Re_b	U_0/U_b
CP	4,000	0.025
CP	4,000	0.05
CP	4,000	0.1
CP	4,000	0.2
CP	5,000	0.025
CP	5,000	0.05
CP	5,000	0.1
CP	5,000	0.2
CP	5,600	0.025
CP	5,600	0.05
CP	5,600	0.1
CP	5,600	0.2
CP	10,000	0.025
CP	10,000	0.05
CP	10,000	0.1
CP	10,000	0.2
CP	15,000	0.025
CP	15,000	0.05
CP	15,000	0.1
CP	15,000	0.2
SIN	4,000	0.1
SIN	5,000	0.1
SIN	5,600	0.1
SIN	10,000	0.1

Figure 3: Percent drag reduction as a function of groove cross-sectional length scale ($\ell_g = \sqrt{A_g}$), in wall units.

11, with subsequent saturation, and drag increase at large Reynolds number and/or riblets size, which is the typical trend of riblets performance also found in experimental studies [2]. Since the rectangular longitudinal bars (Case B) herein considered yield drag increase in all cases, we can regard them as representative of the behavior of rough surfaces, rather than riblets. It should be noted that drag reduction with longitudinal bars was previously reported by several authors [e.g. 8], however with aspect ratio (t/s) less than the present one. The amount of drag reduction for cases $T1 - V0$ and $T1$, namely triangular riblets with and without a slippery interface at the plane of crests (see Fig.2(a) for reference), is very similar for small ℓ_g. However, as a
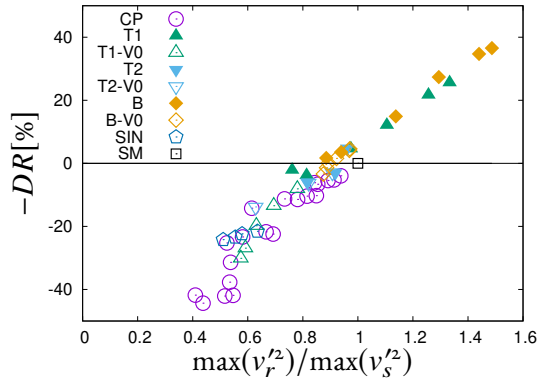
Figure 4: Percent drag reduction versus maximum vertical velocity variance near the lower wall (subscript r), normalized with values at the upper wall (subscript s).

Figure 5: Inner-scaled velocity profiles near the lower wall (lines and symbols) as a function of distance from the plane of crests ($\tilde{y}$). Lines denote the reference log law for low-Re flow, $U^+ = 1/k \log(y^+) + C$, $k = 0.41$, $C = 5.5$.

consequence of the zero wall-normal velocity at the plane of crests, the amount of drag reduction increases with ℓ_g^+ in the former case up to approximately 30%, without saturating as in case $T1$. The same behavior is observed for the $T2 - V0$ and $B - V0$ cases. It is remarkable that longitudinal rectangular bars, yielding drag increase in the baseline case, yield instead drag reducing when vertical velocity at the plane of crests is inhibited. The dependence of DR on ℓ_g^+ is, to a close approximation the same for $T1 - V0$ and $\tilde{T}2 - V0$. This implies that, in the presence of a slippery interface, the amount of drag reduction is mostly affected by the gas fraction, and not by the geometrical features (namely s, h_r and β). Since $T1 - V0$ and $T2 - V0$ outperform $B - V0$, despite having the same gas fraction, it may be deduced that the area fraction (solid/fluid) at the plane of crests is also important, being zero in the former cases, and one half in the latter.

A parametrization for SHS and LIS has been recently proposed by Arenas et al. [1], whereby the drag reduction effect is connected to the ratio of the maximum vertical velocity variance in the vertical direction at the 'rough' wall ($\max(v_r'^2)$) with respect to the 'smooth' wall ($\max(v_s'^2)$). Drag reduction as a function of $\max(v_r'^2)/\max(v_s'^2)$ is shown in Fig. 4. The figure suggests overall linear proportionality in drag-reducing cases, thus extending the results of Arenas et al. [1] also to other surfaces and to a wider range of Reynolds numbers. Deviations from linearity arise for large drag reduction, with a possible lower limit for vertical velocity fluctuations. An interesting finding here is that the linear trend also continues into the rough wall regime, suggesting seamless transition between the two regimes, and the existence of universal mechanisms. Further hints for the universality of this kind of representation also comes from the satisfactory collapse of the Couette-Poiseuille DNS (CP and SIN), although drag reduction seems to be a bit larger than for baseline cases. Based on our extensive database, it appears that substantial friction drag reduction can only be achieved by reducing the intensity of the wall-normal velocity fluctuations.

Fig. 5 shows the inner-scaled mean velocity profiles near the lower wall. While for flow over rough surfaces a virtual
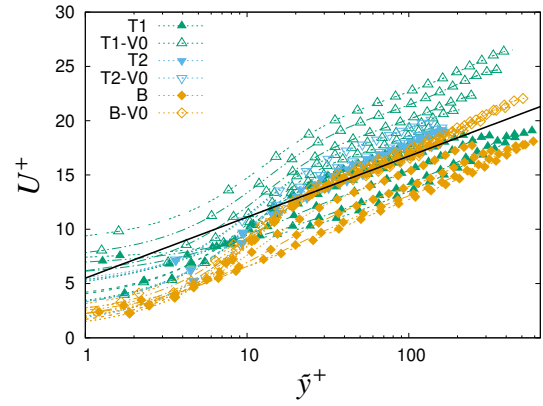
origin is used to account for the heterogeneity of the wall, since the scope of the present paper is to compare a large variety of surfaces, the origin was fixed for all the cases at the plane of crests, and distance from there is denoted as $\tilde{y}$. This also allows for direct comparison with the CP and SIN cases, and with previous numerical simulations in which SHS are modeled as alternating regions with free- and no-slip wall boundary conditions [11, 20]. The mean velocity profiles for cases T1-V0, T2-V0 and B-V0 (the latter only for $Re \geq 10,000$), are shifted above the reference log–law. The upward shift for a given surface is seen to steadily increase with the Reynolds number, consistently with observations made in previous work on SHS and LIS carried out under the assumption of flat slippery and nondeformable interface. In fact, increase of Reynolds number corresponds to increase of the slip length and velocity scaled in wall units, hence to reduction of the wall shear stress. On the other hand, when the vertical velocity at the plane of crests is not forced to be zero (cases T1, T2, B), the velocity profiles are generally shifted downward with respect to the smooth-wall case, by an amount ΔU^+, which is usually referred to as roughness function,

$$U^+ = \frac{1}{\kappa} \log \tilde{y}^+ + C - \Delta U^+. \tag{3}$$

Consistently with previous studies on k-type rough walls [17], we find that the downward shift increases with the Reynolds number.

In Fig. 6 the amount of drag reduction is plotted against the corresponding roughness function, the latter visually estimated by comparing the velocity profiles at the lower and upper walls. Here, negative roughness function indicates upward shift of the velocity profile with respect to that relative to the smooth wall. Strong correlation between the two quantities is found, which implies that the shift in the velocity profiles observed in Fig. 5 is mainly due to the change of the wall shear stress, rather than to a modification of entire organization of turbulence. This further corroborates the work of Rastegari and Akhavan [21], who reported correlation be-
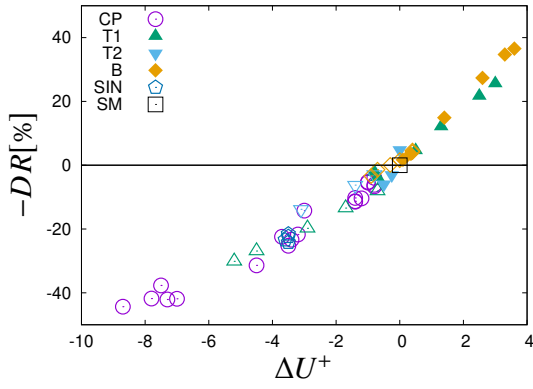
Figure 6: Drag reduction as a function of the roughness function.
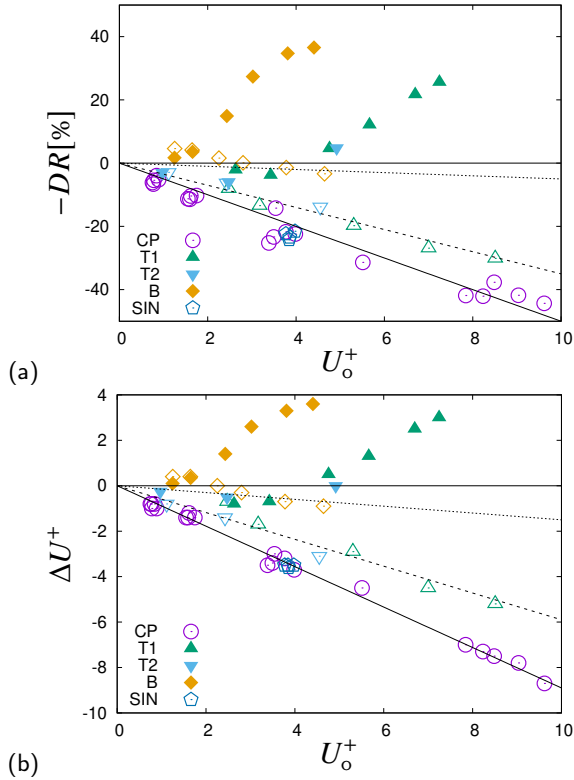

(a)

(b)

Figure 7: Relationship between lower wall slip velocity (U_0) and drag reduction (a), and roughness function (b). Open symbols denote cases with impeded vertical velocity ($V0$).

tween the amount of drag reduction and shift in the log-law intercept. Fig. 6 shows that the relation between the amount of drag reduction and ΔU^+ is universal to a close approximation, reconciling both drag-increasing and drag-reducing surfaces, and regardless of the Reynolds number.

The data in Fig. 3 and 5 suggest proportionality between slip velocity and drag reduction effect for the CP, SIN, T1-V0 and T2-V0 cases This is consistent with the studies of Rastegari and Akhavan [20], who reported

$$DR = \frac{U_0}{U_b} + o(\epsilon), \tag{4}$$

where U_0 is the slip velocity, and $o(\epsilon)$ accounts for the tur-

bulent structures and secondary motions. The same relationship can be expressed as a function of U_0^+, as it easily results out from Eq. 4. For each surface the amount of drag reduction varies linearly with the slip velocity normalised in wall units, regardless of the Reynolds number, as shown in Fig. 7(a), however with slope varying from case to case. For a given slip velocity, the CP and SIN cases yield the largest drag reduction (and largest slope). The slope is slightly smaller for triangular riblets with slippery interface (T1-V0 and T2-V0), and significantly reduced for the B-V0 case. On the other hand, linearity between DR and U_0^+ is not found in the case of rough walls, and the trend is opposite. This is due to the term $o(\epsilon)$ in Eq. 4 which overcomes the reduction of the shear associated with the presence of a slip velocity. Indeed, the contribution of the form drag, which is proportional to the square of the slip velocity, is dominant in the momentum balance [10, 6].

In Fig. 7(b) we show the roughness function plotted against the mean slip velocity. Interestingly we find that, for given riblet geometry, a linear relationship is present, namely $\Delta U^+ \approx \alpha U_0^+$, with geometry-dependent slope, which persists in all DNS with suppression of vertical velocity, and which it is lost in the case of standard no-slip boundary condition past the performance breakdown point. The slope is seen to increase from $\alpha = 0.15$ for square bars, to about $\alpha = 0.59$ for triangular riblets, reaching the highest value $\alpha = 0.89$ for CP flow cases. Quite surprisingly, we find that the case with sinusoidal slip velocity (SIN) has the same performance as the CP case in which the imposed wall velocity is uniform velocity. Hence, spanwise modulation of the slip velocity has little effect on drag reduction, somewhat in line with the study of Busse and Sandham [3], who concluded that any coupling between streamwise and spanwise slip does not have strong influence on drag. Differences in α across cases with vertical velocity suppression and with CP cases, with associated different drag-reduction efficiency lead us to conclude that, also in those cases the texture geometry and the flow inside the grooves is important. In fact, although there is no mass communication between the bulk flow and the flow within the grooves, the latter is driven by viscous shear at the plane of crests. From a practical standpoint, it appears that the influence of the wall geometry can be distilled into the single parameter α, which may be determined for any given riblet geometry, once and for all.

The empirically determined relationship between ΔU^+ and U_0^+ can be profitably exploited to derive an analytical expression for the friction coefficient as a function of the bulk Reynolds number. For that purpose, we preliminarily introduce an effective height (h_e), as the difference between the point at which total stress is zero and the plane of crests ($y = y_0$), and an effective bulk velocity (U_{be}) in terms of the associated mass flow rate, namely

$$U_{be} = \frac{1}{h_e} \int_{y_0}^{h_e} U(y) \mathrm{d}y. \tag{5}$$

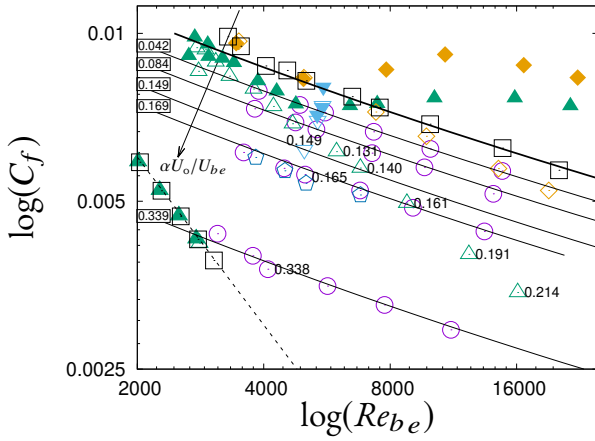As for smooth channels, assuming that the mean velocity

Figure 8: Friction coefficient as a function of bulk Reynolds number for SM ($\square$), T1 ($\blacktriangle$), T1-V0 ($\triangle$), T2 ($\blacktriangledown$), T2-V0 ($\triangledown$), B ($\blacklozenge$), B-V0 ($\lozenge$), CP ($\bigcirc$), SIN ($\varhexagon$). The solid black lines denote the analytical predictions of Eq. (8), for $\alpha U_0/U_{be} = 0, 0.042, 0.084, 0.149, 0.169, 0.339$ (from top to bottom). The dashed line denotes the friction law for laminar flow, $C_f = 12/Re_b$. Representative DNS are also labeled with the corresponding value of $\alpha U_0/U_{be}$.

Figure 9: Wall-normal distributions of Reynolds stress components [13].

profile obeys a logarithmic law throughout,

$$U^+ = \frac{1}{k}\log y^+ + C - \Delta U^+ \approx \frac{1}{k}\log y^+ + C - \alpha U_0^+, \quad (6)$$

and integrating in the vertical direction, one easily obtains

$$\sqrt{\frac{C_{fb}}{2}}\left(1 + \alpha\frac{U_0}{U_{be}}\right) + \frac{1}{k}\log\left(2\sqrt{\frac{C_{fb}}{2}}\right) = \quad (7)$$

$$\frac{1}{k}\left(\log(Re_{be} - 1)\right) + C, \quad (8)$$

whence the friction coefficient $C_f = 2/U_{be}^{+2}$ can be numerically obtained as a function of Re_{be} and U_0/U_{be}. It is also a simple matter to show that in the case of laminar flow

$$C_f = \frac{12}{Re_{be}}\left(1 - \frac{U_0}{U_{be}}\right). \quad (9)$$

Fig. 8(b) shows the friction coefficient versus the bulk Reynolds number as obtained from all DNS herein reported. The analytical trends predicted from Eq. (8) are also reported for increasing values of $\alpha U_0/U_b$ (solid lines), corresponding to drag reduction with respect to the smooth channel case, to obtain a Moody-like diagram. As expected, the behavior of friction in smooth channels (SM) is well reproduced from the laminar into the turbulent regime, with transition occurring between $Re = 3,000$ and $Re = 3,250$. As for the CP flow cases, they all show excellent agreement with the theoretical predictions, namely they all reside with minimal scatter, on the C_f curve corresponding to the respective $\alpha U_0/U_b$. Similar considerations can be made for the SIN cases, which are also found where predicted. Analyzing the behavior of riblets, some drag reduction is observed
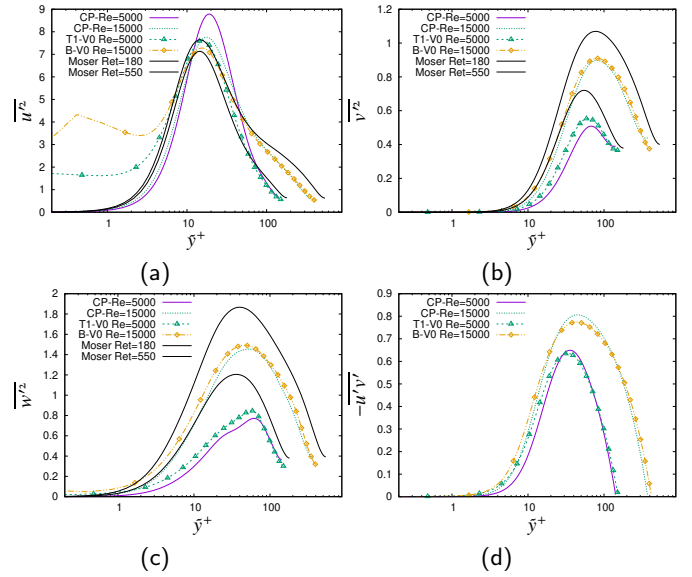
at transitional Reynolds numbers, with no substantial difference between non-slip and slip boundary conditions. Classical riblets are found to reach optimal performance for a specific number of Reynolds, past which they show increase and saturation of the friction coefficient in the fully rough regime. On the other hand the $V0$ simulations show a continuing trend for C_f to decrease with Re_b, at a rate which is well parametrized by Eq. (8). Once again, Fig. 8 confirms that uniform slip velocity, which may be thought as a moving wall (CP) is the most efficient way for achieving drag reduction through wall slip.

3.2. Turbulence structure

In order to understand the reduced efficiency of riblets with slippery interface with respect to the case with imposed slip velocity, in Fig. 9 we compare the corresponding distributions of the Reynolds stress components. No substantial difference is found between the vertical and spanwise velocity fluctuations in riblets and CP flows. On the other hand, large differences are found toward the plane of crests in the streamwise velocity variance, which is quite large in riblets, and obviously zero in CP flow. Hence, we conjecture that poorer performance of riblets with impeded vertical velocity with respect to CP flows is related to higher turbulent kinetic energy at the plane of crests, which must be sustained through additional power expenditure.

This is further corroborated by comparing the budgets of vertical velocity fluctuations for the T1 (Fig. 10a) and T1-V0 (Fig. 10b) flow cases, at $Re = 15,000$. The shape of the texture is the same ($T1$) however, because of the impermeable interface the latter yields a reduction of the drag, whereas the former yields drag increase. The figure well highlights that drag reduction through suppression of vertical velocity does not qualitatively change the wall-layer dynamics compared with the smooth wall case. However, drag reduction is
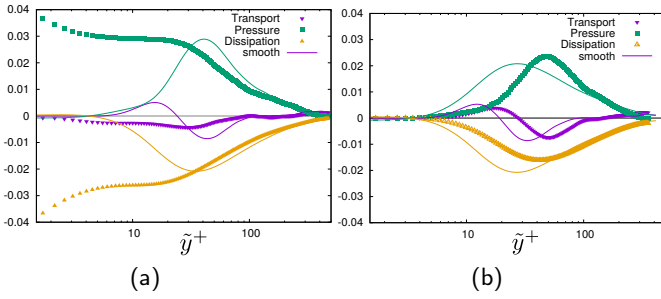
(a)   (b)

Figure 10: Budgets of vertical velocity variance for triangular riblets at $Re = 15,000$ (T1, panel (a)), and with suppression of vertical velocity at the plane of crests ($T1 - V0$, panel (b)). Effective dissipation, $-\nu\langle v'\nabla^2 v'\rangle$; turbulent transport, $-\mathrm{d}\langle v'^3\rangle/\mathrm{d}y$; pressure, $-2\langle v'\partial p'/\partial y\rangle$. The thin solid lines depict budget terms near the upper, smooth wall.
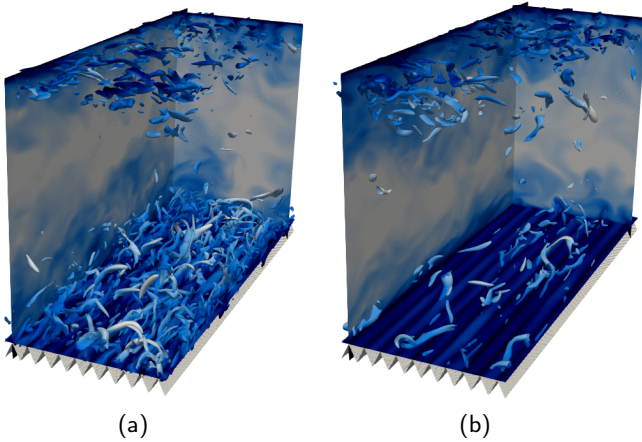

(a)   (b)

Figure 11: Q-criterion iso-surfaces and streamwise velocity contours for a) $T1$ case and b) $T1 - V0$ case, both at $Re = 15,000$. The iso-surfaces are generated for $Q = 3$.

accompanied by proportionate reduction of all budget terms, and by outward shift of the pressure and dissipation peaks. On the other hand, drag increase is a associated with disruption of the wall layer organization. In particular, the pressure term is now maximum at the plane of crests, highlighting the importance of mechanism of kinetic energy transfer from the longitudinal component to the vertical one. As a result, dissipation is also greatly enhanced across the whole wall layer.

These structural changes can also be appreciated in instantaneous flow visualizations. In Fig. 11 we show turbulent structures through iso-surfaces of the flow discriminant (Q criterion), for T1 simulations at $Re = 15,000$. Comparing cases with and without vertical velocity suppression, it appears that drag increase is associated with larger number of turbulent structures as compared to the upper wall (see panel (a)), whereas drag reduction is accompanied by reduced number of turbulent structures (see panel (b)).

Insights for wall modeling of riblets and SHS/LIS surfaces may be obtained from inspection of the streamwise and spanwise velocity fields at the plane of crests, and comparison with their vertical gradients. Contours of these quantities are shown are shown in Fig. 12 and 13 for the B and
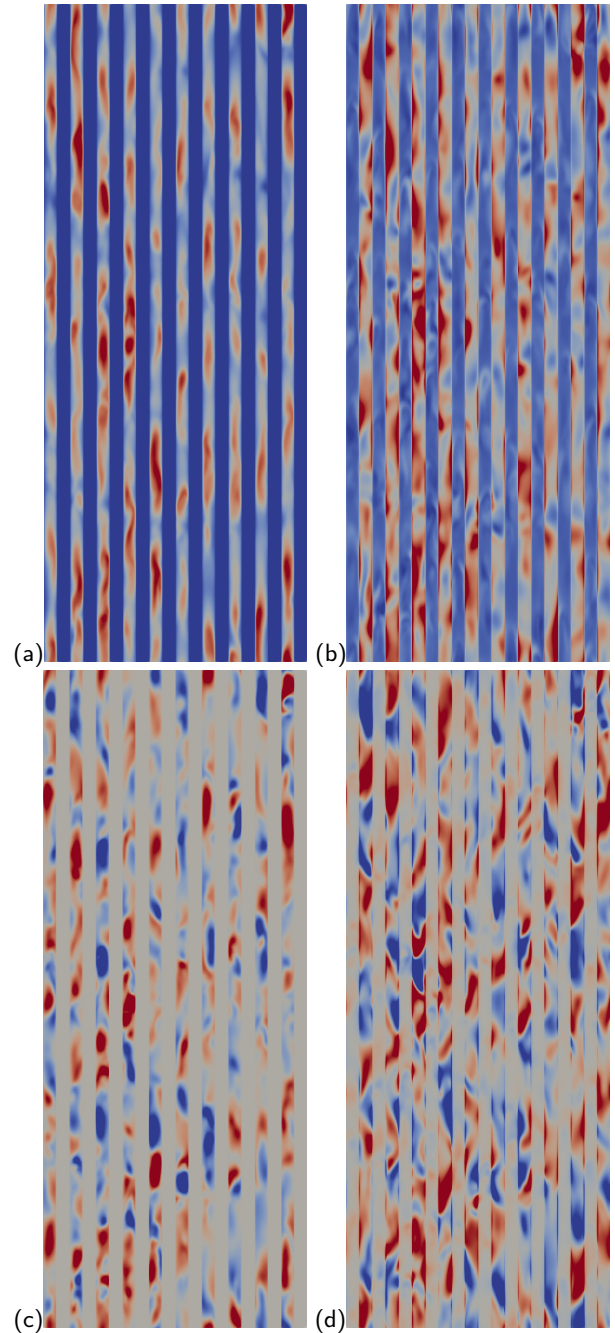

Figure 12: Flow properties in $x-z$ plane at the riblets crest for B simulation at $Re = 15,000$. a) streamwise velocity U, b) vertical streamwise velocity gradient $\partial U/\partial y$, c) Instantaneous spanwise velocity W, d) vertical spanwise velocity gradient $\partial W/\partial y$.

$B - V0$ cases, corresponding to a state of drag increase and drag reduction, respectively. Besides the obvious observation that U and W are zero at the edge of the bars, we see that both the U and the W streaks are longer in the $B - V0$ case. Patterns of $\partial U/\partial y$ have similar length, but close inspection shows no clear hint of association with U. On the other hand, the vertical gradient of W has a similar distribution as W itself. This association is made clearer in fig-

(a) (b)

(c) (d)

Figure 14: Joint PDF at the plane of crests between U and $\partial U/\partial y$ (a, b) and between W and $\partial W/\partial y$ (c, d), for cases B (a, c) and $B - V0$ (b, d), at $Re = 15,000$.
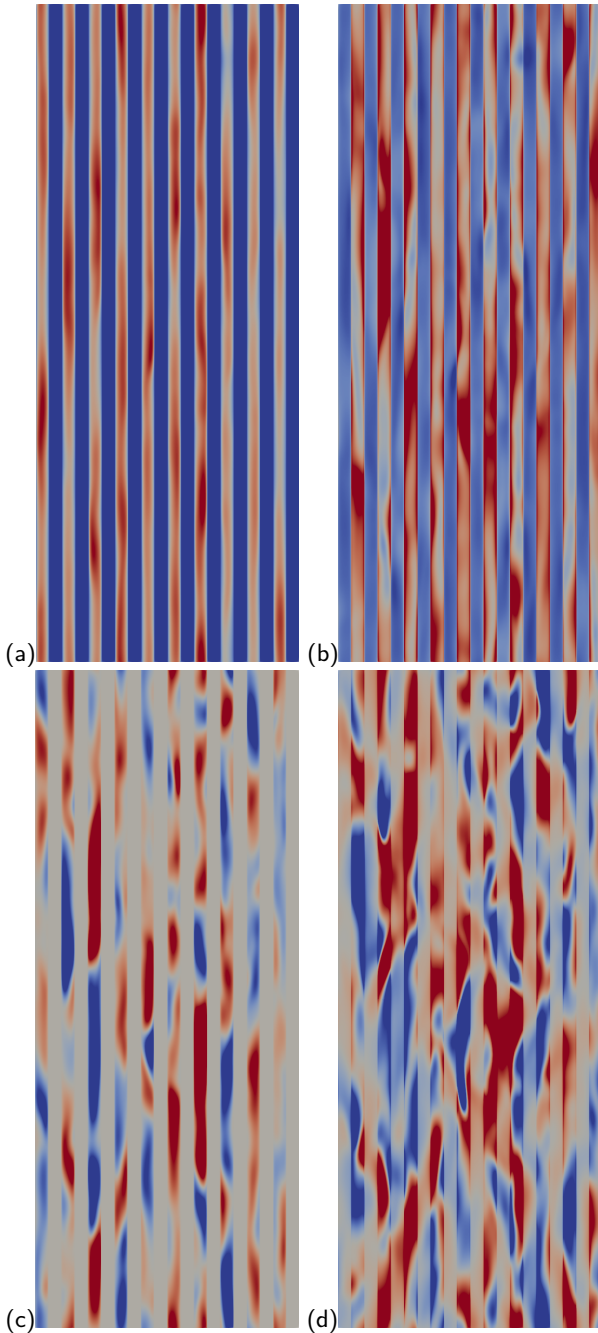

(a) (b)

(c) (d)

Figure 13: Flow properties in $x - z$ plane at the riblets crest for $B - V0$ simulation at $Re = 15,000$. a) streamwise velocity U, b) vertical streamwise velocity gradient $\partial U/\partial y$, c) Instantaneous spanwise velocity W, d) vertical spanwise velocity gradient $\partial W/\partial y$.

ure 14, where we show the joint PDF between the velocity components and the corresponding vertical gradients. Although gradients are obviously larger for the case without vertical velocity impedance, the qualitative behavior is similar in the two cases. Regarding the streamwise velocity, the vertical band corresponds to the edges of the bars where $U = 0$, and the small diagonal band corresponds to the first grid point outside the bar. Most of the flow over the grooves
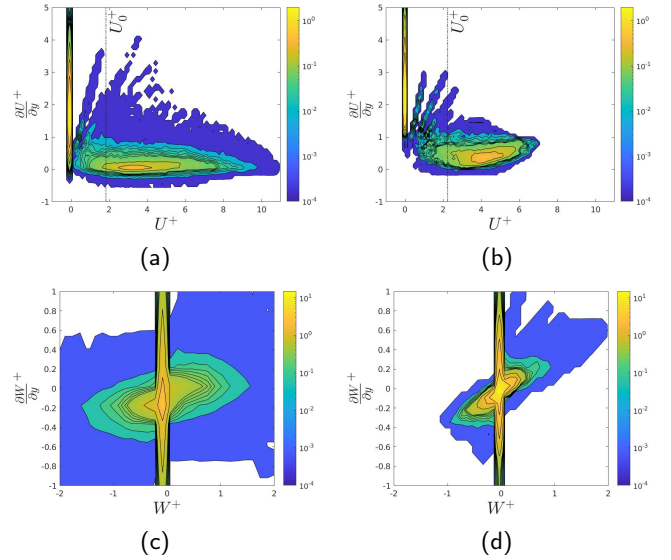
however is characterized by the absence of any clear relationship between U and its vertical gradient, and in fact $\partial U/\partial y$ is probably even reducing at large U. The joint PDF of the spanwise velocity shows the same vertical band, however it additionally features the presence of a diagonal band which is the signature of the previously noted association between W and its vertical gradient. Similar results, not shown, also apply to the other cases which we have numerically simulated. This is an evidence that SHS/LIS cannot be reliably simulated using simplified wall models as those based on the use of a slip length, but rather simulating the actual underlying riblets geometry is important, especially in the case of high Reynolds number and/or large riblets. The present data in fact show no evidence for proportionality between local longitudinal velocity and shear, hence no slip length can be reasonably defined for the streamwise direction. This conclusion does not apply to the spanwise velocity component, which instead seems to be approximately characterizable in terms of a spanwise slip length.

Further insight into the flow behavior at the plane of crests is provided in Fig. 15, where we show the standardized probability density functions (PDF) of the vertical velocity gradient. The SM and CP cases are also shown for comparison, with data evaluated at the wall. Two PDFs are shown separately for points at the edge of the bars (panel (a)) and over the grooves (panel (b)). First, we note that no difference exists between the case of smooth steady wall (SM) and of moving wall (CP), in agreement with the findings of Pirozzoli et al. [18]. In both cases, the PDFs are positively skewed, as sweep events are most intense underneath the buffer layer [9]. Rectangular bars have similar behavior for sampling points placed over their edge, although looking carefully the B case shows slightly greater probability of intense events with both positive negative shear fluctua-
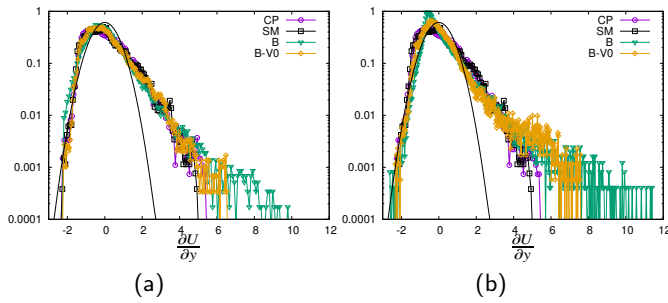
Figure 15: PDF of standardized vertical gradient of streamwise velocity. Data are collected at the lower wall for the SM and CP simulations, and at the plane of crests for the B and $B−V0$ simulations, separately at the edge of the bars (a), and over the grooves (b). The solid lines denotes the standard Gaussian distribution.

tions. Larger differences emerge when the sampling point is placed over the grooves, in which case events with positive and negative deviations of about one-two standard deviations are suppressed, in favor of events with small, negative fluctuations. Apparently, removing the wall yields reduction of the flow intermittency.

4. Conclusion

Direct numerical simulations of a turbulent channel flow with either triangular or rectangular riblets on the lower wall have been performed for a wide range of Reynolds number. Two sets of simulations have been carried out, with and without suppression of the vertical velocity at the plane of crests to assess differences between classical riblets or rough walls and LIS (under idealized conditions of infinite surface tension). In addition, DNS with prescribed wall slip velocity wall have been performed and used as reference to analyze how the flow is affected by the shape of the textures. Consistent with previous studies, drag reduction of up to 9% is achieved with traditional riblets for $\ell_g^+ = \sqrt{A_g} \approx 11$, where A_g is the grooves area. This considerably limits their practical application for Reynolds numbers of engineering interest. On the other hand, LIS can reduce the drag up to 30% thanks to suppression of the wall-normal velocity fluctuations near the wall. In fact, we have found very strong correlation between the maximum of the wall normal velocity fluctuations and the amount of drag reduction, which further corroborates previous work of Arenas et al. and Orlandi. Based on our extensive database, it appears that substantial friction drag reduction can only be achieved by reducing the intensity of the wall-normal velocity fluctuations. We also found strong relation between the amount of drag reduction and the roughness function, which reconciles both drag-increasing and drag-reducing surfaces, regardless of the Reynolds number.

In line with previous work on SHS/LIS, we also find clear association between the amount of drag reduction and the presence of a slip velocity. In this respect, we have two interesting findings: i) in the case of a flat wall with imposed

slip velocity (CP and SIN cases), the actual spatial distribution of the slip velocity is not important, and the amount of drag reduction only depends only its mean value; ii) in the presence of riblets with suppressed vertical velocity at the plane of crests, drag reduction is less than in the case of a flat wall, also with the same slip velocity. We speculate that this is related to higher turbulent kinetic energy at the plane of crests, which must be sustained through additional power loss. Hence, the shape of the surface and the flow within the grooves cannot be simply taken into account through a simple slip velocity wall boundary condition. This is further proved by visualizations and statistics of the instantaneous streamwise velocity and its vertical gradient. In fact, the present data show no evidence for proportionality between local longitudinal velocity and shear, hence no slip length can be reasonably defined for the streamwise direction. This conclusion does not apply to the spanwise velocity component, which instead seems to be approximately characterizable in terms of a spanwise slip length.

Expanding on the work of Rastegari and Akhavan, we find that for any given texture a nearly linear relationship exists between the roughness function and the slip velocity, namely $\Delta U^+ = \alpha U_0^+$, where the slope α depends on the shape of the texture. The influence of the wall geometry can be thus reduced into the single parameter α, which may be determined for any given surface, once and for all. We have used this novel parametrization to obtain a Moody-like chart whereby the variation of the friction coefficient with the bulk Reynolds number is characterized, for any assigned value of the parameter $\alpha U_0/U_b$. This findings can in perspective be leveraged to evaluate the drag-reducing performance of different textures.

Regarding the structure of turbulence, we find that drag reduction is accompanied by proportionate reduction of all terms in the balance of the vertical velocity variance, and by outward shift of the pressure and dissipation peaks, but the same qualitative organization as for the case of smooth walls is retained. On the other hand, drag increase over rough walls is associated with disruption of the entire wall layer organization. In particular, the pressure term is maximum at the plane of crests, highlighting the importance of mechanism of kinetic energy transfer from the longitudinal component to the vertical one (which in fact is inhibited by the interface in LIS). This is in striking contrast to the case of wall actuation through spanwise wall oscillation [19], whereby drag reduction is achieved by disrupting the near-wall streaks, thus achieving large drag reduction.

References

[1] Arenas, I., Garciá, E., Fu, M.K., Orlandi, P., Hultmark, M., Leonardi, S., 2019. Comparison between super-hydrophobic, liquid infused and rough surfaces: A direct numerical simulation study. J. Fluid Mech. 869, 500–525. doi:10.1017/jfm.2019.222, arXiv:1812.05674.

[2] Bechert, D.W., Bruse, M., Hage, W., Van Der Hoeven, J.G., Hoppe, G., 1997. Experiments on drag-reducing surfaces and their optimization with an adjustable geometry. J. Fluid Mech. 338, 59–87. doi:10.1017/S0022112096004673.

[3] Busse, A., Sandham, N.D., 2012. Influence of an anisotropic slip-

length boundary condition on turbulent channel flow. Phys. Fluids 24. doi:10.1063/1.4719780.

[4] Choi, H., Moin, P., Kim, J., 1993. Direct numerical simulation of turbulent flow over riblets. J. Fluid Mech. 255, 503–539. doi:10.1017/S0022112093002575.

[5] Fukagata, K., Kasagi, N., Koumoutsakos, P., 2006. A theoretical prediction of friction drag reduction in turbulent flow by superhydrophobic surfaces. Phys. Fluids 18, 16–20. doi:10.1063/1.2205307.

[6] García-Cartagena, E.J., Arenas, I., An, J., Leonardi, S., 2019. Dependence of the drag over superhydrophobic and liquid infused surfaces on the asperities of the substrate. Phys. Rev. Fluids 4, 114604. URL: https://link.aps.org/doi/10.1103/PhysRevFluids.4.114604, doi:10.1103/PhysRevFluids.4.114604.

[7] García-Mayoral, R., Jiménez, J., 2011. Drag reduction by riblets. Philos. T. Roy. Soc. A. 369, 1412–1427. URL: http://rsta.royalsocietypublishing.org/content/369/1940/1412, doi:10.1098/rsta.2010.0359.

[8] García-Mayoral, R., Jiménez, J., 2012. Scaling of turbulent structures in riblet channels up to $Re_\tau \approx 550$. Phys. Fluids 24, 105101. URL: https://doi.org/10.1063/1.4757669, doi:10.1063/1.4757669.

[9] Kim, J., Moin, P., Moser, R., 1987. Turbulence statistics in fully developed channel flow at low Reynolds number. J. Fluid Mech. 177, 133–166.

[10] Leonardi, S., Orlandi, P., Smalley, R.J., Djenisi, L., Antonia, R.A., 2003. Direct numerical simulations of turbulent channel flow with transverse square bars on one wall. J. Fluid Mech. 491, 229–238. doi:10.1017/S0022112003005500.

[11] Martell, M.B., Perot, J.B., Rothstein, J.P., 2009. Direct numerical simulations of turbulent flows over superhydrophobic surfaces. J. Fluid Mech. 620, 31–41. doi:10.1017/S0022112008004916.

[12] Min, T., Kim, J., 2004. Effects of hydrophobic surface on skin-friction drag. Phys. Fluids 16, L55–L58. URL: https://doi.org/10.1063/1.1755723, doi:10.1063/1.1755723, arXiv:https://doi.org/10.1063/1.1755723.

[13] Moser, R.D., Kim, J., Mansour, N.N., 1999. Direct numerical simulation of turbulent channel flow up to $Re_\tau = 590$. Phys. Fluids 11, 943–945. URL: https://doi.org/10.1063/1.869966, doi:10.1063/1.869966, arXiv:https://doi.org/10.1063/1.869966.

[14] Orlandi, P., 2012. Fluid flow phenomena: a numerical toolkit. volume 55. Springer Science & Business Media.

[15] Orlandi, P., Leonardi, S., 2006. DNS of turbulent channel flows with two-and three-dimensional roughness. J. Turbul. , N73.

[16] Orlandi, P., Leonardi, S., 2008. Direct numerical simulation of three-dimensional turbulent rough channels: parameterization and flow physics. J. Fluid Mech. 606, 399–415. doi:10.1017/S0022112008001985.

[17] Perry, A.E., Schofield, W.H., Joubert, P.N., 1969. Rough wall turbulent boundary layers. J. Fluid Mech. 37, 383–413. doi:10.1017/S0022112069000619.

[18] Pirozzoli, S., Bernardini, M., Orlandi, P., 2011. Large-scale organization and inner-outer layer interactions in turbulent Couette-Poiseuille flows. J. Fluid Mech. 680. 534-563.

[19] Quadrio, M., 2011. Drag reduction in turbulent boundary layers by in-plane wall motion. Philos. T. Roy. Soc. A. 369, 1428–1442.

[20] Rastegari, A., Akhavan, R., 2015. On the mechanism of turbulent drag reduction with super-hydrophobic surfaces. J. Fluid Mech. 773, R4.1–R4.14. doi:10.1017/jfm.2015.266.

[21] Rastegari, A., Akhavan, R., 2019. On drag reduction scaling and sustainability bounds of superhydrophobic surfaces in high Reynolds number turbulent flows. J. Fluid Mech. 864, 327–347. doi:10.1017/jfm.2018.1027.

[22] Walsh, M.J., 1986. Riblets for aircraft skin-friction reduction. Technical Report. NASA Langley Research Center, Hampton, VA, United States).